High-Performance Nanopapers Based on Benzenesulfonic Functionalized Graphenes

Wenyi Huang, Xilian Ouyang, and L. James Lee*

Department of Chemical and Biomolecular Engineering, The Ohio State University, Columbus, Ohio 43210, United States

ABSTRACT High-performance graphene nanopapers are prepared from an aqueous solution of functional graphenes with benzenesulfonic acid groups *via* covalent bonds. The formed hydrophobic graphene nanopapers showed the highest tensile strength of 360 MPa and Young's modulus of 102 GPa for samples with 13.7 wt % functional group and annealed at 150 °C. These samples showed a high electrical conductivity of 4.45 × 10^4 S/m after being annealed at 250 °C. The aforementioned properties of graphene nanopapers are much higher than any previously reported data. The properties of nanopapers depend on the degree of functionality on graphenes and the annealing temperatures, which are further evidenced by X-ray photoelectron spectroscopy, FTIR, and X-ray diffraction patterns. Such unique nanopapers can be easily bounded and sandwiched onto any solid surface to give rise to great potentials in many applications such as gas diffusion barriers, EMI shielding, thermal management, and anticorrosion.

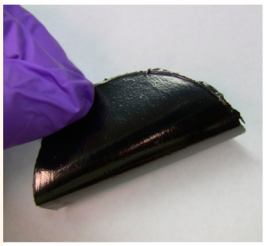

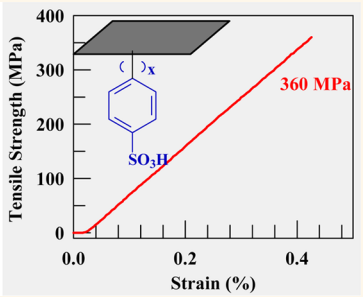

KEYWORDS: functional graphenes · nanopapers · mechanical properties · electrical conductivity · X-ray

Nanopapers are often referred to as thin sheets or films made of nanomaterials such as carbon nanotubes,[1,2] carbon nanofibers,[3] nanoclays,[4] cellulose nanofibrils,[5] and more recently graphene nanoplatelets.[6,7] Noticeably, nanopapers allow highly concentrated nanoparticles to be tightly packed in a thin film to reach unique properties such as very high electrical and thermal conductivities, very low gas diffusivity, and strong corrosion resistance that are not shared by conventional polymer nanocomposites,[8,9] where the loading of nanoparticles is very limited because of dispersion issues. Among these, graphene is of particular interest because this one-atom-thick planar sheet with sp^2 hybridized carbon possesses ultrahigh strength,[10] superior electrical[11] and thermal conductivity,[12] and an extremely high surface area.[13] These unique features allow graphene to stand out as an ideal nanomaterial for fabricating high-performance nanopapers.

To achieve graphene nanopapers with superior properties, two prerequisites must be satisfied: the exfoliation and good dispersion of individual graphene nanosheets in a medium and the strong bonding among graphene nanosheets in the resulting nanopapers. The seminal work of Ruoff *et al.*[14] on graphene oxide (GO) nanopapers lies in the fact that GO can be well exfoliated in water by ultrasonication owing to its hydrophilic nature, and then processed into nanopapers through flow-directed assembly of individual GO nanosheets during filtration. The resulting GO nanopapers have a decent tensile strength around 40 MPa and Young's modulus around 32 GPa, but they are electrically insulated. When the hydrophilic GO in the aqueous solution is reduced into hydrophobic graphene using reducing agents, restacking of graphene nanosheets is inescapable, and the resulting aggregates are hard to redisperse in water or organic solvents.[15] For this reason, surfactants or water-soluble polymers are often employed to overcome the problem of restacking,[16,17] but it is rather difficult to completely remove them from the graphene surface upon the formation of nanopapers and consequently the mechanical and electrical properties of nanopapers suffer.[18,19] For this reason, ammonia was wisely employed as the electrostatic

* Address correspondence to lee.31@osu.edu.

Received for review August 26, 2012 and accepted October 25, 2012.

Published online October 25, 2012
10.1021/nn303917p

© 2012 American Chemical Society

TABLE 1. The Concentration of Functional Groups, Degree of Functionality per 100 Carbons, Zeta Potentials, and Contact Angle of GP−SO_3H under Different Reaction Conditions

GO/diazonium molar ratio	10/1	5/1	1/1	1/2
concentration of functional group (wt %)[a]	10.6	13.7	16.8	22.4
degree of functionality (DS) per 100 carbons	0.90	1.21	1.54	2.21
zeta potential (mV) at pH = 7	−30.93 ± 3.12	−34.88 ± 2.03	−45.34 ± 2.46	−56.86 ± 3.38
contact angle (degree)[b]	84.6	77.9	59.4	26.7

[a] Determined by thermogravimetric analysis in Figure S2. [b] After annealing at 150 °C in vacuum for 24 h to remove the entrapped water.

stabilizer to achieve stable graphene colloids, which could be processed into nanopapers with the highest reported tensile strength of 293.3 MPa and an electrical conductivity of 3200 S/m at room temperature.[20] However, the resulting graphenes are only partially reduced due to the insufficient hydrazine used, and also the high volatility of ammonia represents a major obstacle for the scale-up of this process. More recently, graphene oxide was processed into fibers and then thermally treated at 800 °C, giving rise to a tensile strength of 420 MPa and an electrical conductivity of about 1000 S/m in the final product.[21] Up to now, the great potential of graphene is far from fully exploited in nanopapers, and thus it is imperative to develop a reliable approach to achieve large-scale production for stable graphene colloids and strong bonding in the resulted nanopapers.

Herein we present a facile method to achieve high performance graphene nanopapers by covalently functionalizing the graphene surface with a controllable amount of negatively repulsive groups (*i.e.*, benzenesulfonic acid) in such a way that the obtained functional graphene can be well dispersed in water and is capable of fabricating into nanopapers in an environmentally friendly manner. Through a systematic study, we have finely tuned the degree of functionality and processing conditions to achieve graphene nanopapers with the highest mechanical and electrical properties ever documented in the literature and yet with excellent stability in a humid environment.

RESULTS AND DISCUSSION

Functional graphenes (GP−SO_3H) were synthesized according to literature in an improved manner.[22] The detailed reaction scheme is given in Figure S1 of Supporting Information. Specifically, expanded graphite was oxidized into graphite oxide *via* the Staudenmaier method.[23,24] Graphite oxide was then exfoliated into graphene oxide (GO) in water under sonication, followed by partial reduction by sodium borohydride. The partially reduced graphene oxide remained soluble in water while the recovered conjugated structure was able to react *via* reductive coupling[25,26] with 4-sulfonic acid phenyl diazonium tetrafluoroborate to form GO−SO_3H. Tetrafluoroborate diazonium salt is stable at room temperature and therefore is much easier to purify and handle than chloride diazonium salt that is only stable at 0 °C,[22] an important consideration for large-scale synthesis of functional graphenes. Finally, GO−SO_3H was fully reduced into GP−SO_3H by hydrazine with a hydrazine to GO−SO_3H weight ratio of 12.8:1. Because of the existence of sulfonic acid groups on the surface of graphenes, GP−SO_3H showed excellent dispersion in water and then hydrazine was able to reach each single-layer graphene surface to conduct complete reduction. This is an essential part toward the preparation of high-performance graphene nanopapers. Since GP−SO_3H could be homogeneously dispersed in water, high-quality graphene nanopapers were prepared by filtration of the aqueous solution of graphene nanosheets through a polycarbonate membrane filter.

The degree of functionality in GP−SO_3H is closely associated with the amount of 4-sulfonic acid phenyl diazonium tetrafluoroborate used for reductive coupling, as illustrated in Table 1. That is, a higher loading of diazonium salt provides a higher weight percentage of functional group in GP−SO_3H, and thus a higher degree of functionality (DS) per 100 carbons, thereby leading to a larger zeta potential in water and a smaller water contact angle on nanopapers. A higher degree of functionality in GP−SO_3H gives rise to better graphene dispersion in water; for example, the solubility of GP−SO_3H with DS = 0.9 is about 0.2 mg/mL, while that with DS = 2.21 is approximately 6 mg/mL. However, an excessive amount of functional groups in GP−SO_3H (*e.g.*, DS = 1.54 or 2.21) leads to poor stability of nanopapers in humid environment. We have found out that GP−SO_3H nanopapers with DS = 0.9 or 1.21 were very stable in humid atmosphere after being annealed at 150 °C to remove the entrapped water. Furthermore, the hydrophobicity of nanopapers could be greatly improved when the nanopapers underwent thermal treatment at an elevated temperature. For instance, the contact angle for GP−SO_3H nanopaper with DS = 0.9 was increased by 13.6° when the annealing temperature was raised from 150 to 250 °C (Supporting Information, Figure S3). Note that its mechanical properties remained the same after soaking in water for 4 weeks. The mechanism behind these will be elaborated on by structural characterizations.

The ^{1}H NMR spectrum in Figure 1a verifies the presence of phenyl groups in the graphene nanosheets with the following chemical shifts (250 MHz, D_2O-d_2, δ/ppm): 7.67 (d, J = 8.0 Hz, 2H, Ar−H), 7.42 (d, J = 6.75 Hz, 2H, Ar−H). In contrast, the precursor monomer, 4-sulfonic

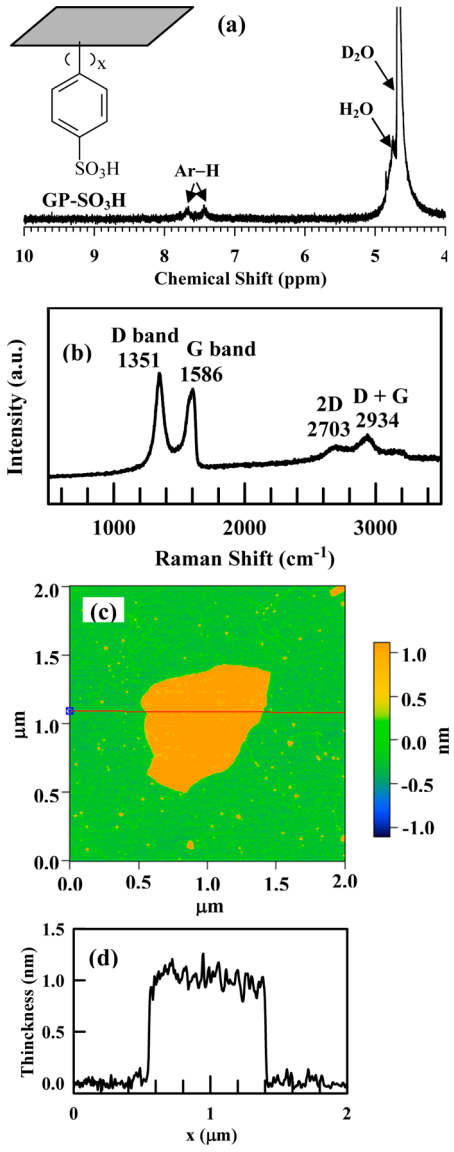

Figure 1. (a) ^{1}H NMR spectrum of GP−SO_3H in D_2O and the inset gives its chemical structure, (b) Raman spectrum of GP−SO_3H nanopaper, (c) AFM image of monolayer GP−SO_3H, and (d) height profile indicated by the red line in the AFM image.

acid phenyl diazonium tetrafluoroborate, shows higher chemical shifts at 8.64 (d, J = 8.5 Hz, 2H, Ar−H) and 8.10 (d, J = 8.5 Hz, 2H, Ar−H), due to the influence of diazonium salt. It can be observed from Raman spectrum in Figure 1b that GP−SO_3H has a G band at 1586 cm^{-1} and a D band at 1351 cm^{-1}. The integrated intensity ratio (I_D/I_G) of the D band and G band for GP−SO_3H nanopaper is 1.3, which is significantly larger than that of expanded graphite (0.003) (Supporting Information, Figure S5).[27] The increased I_D/I_G ratio of GP−SO_3H nanopaper is the combined consequence of the formation of the sp^3 nodes on the graphene basal plane after functionalization and the sp^3 hybridized carbon in benzenesulfonic groups. The 2D band for GP−SO_3H nanopapers resides at 2703 cm^{-1}, indicative of the sp^2 network being present within nanosheets.[28,29]

The successful attachment of benzenesulfonic groups onto graphene *via* covalent bonds facilitates the dispersion of GP−SO_3H in water as a single layer, which is confirmed by an AFM image in Figure 1c. As shown in Figure 1d, the average thickness of graphene nanosheets is about 1.06 nm, which is consistent with the theoretical calculation in Supporting Information, Figure S4 and supports the existence of single layers.

Because of the strong repulsive force of −SO_3H in GP−SO_3H, about one functional group per 100 carbons is sufficient for achieving its good dispersion in water. Most of graphene surfaces still have a great chance to form $\pi-\pi$ interactions, producing a strong bonding force inside the nanopapers. As a result, the tensile strength of our nanopapers with 13.7 wt % functional group after being annealed at 150 °C can reach a value as high as 360 MPa (Figure 2a), very close to that of structural steel and 10 times higher than that of GO. Referring to SEM images in Figure 3, GP−SO_3H nanosheets are packed much more tightly than GO nanosheets in the nanopapers. It should be noticed that the density of steel is 7.8 g/cm^3, while the density of our nanopaper having 13.7 wt % functional group after being annealed at 200 °C is only about 1.72 g/cm^3. Figure 2b reveals that the tensile strength of graphene nanopapers highly depends on the concentration of functional groups, and it goes through a maximum at 13.7 wt %, where both good dispersion of graphenes in water and strong interlayer bonds inside the resulted nanopapers are achievable. An excessive amount of functional groups would result in a larger gallery distance and consequently lead to the reduced interlayer $\pi-\pi$ interactions, whereas a lower amount of functional groups would not afford good dispersion of graphene in water.

Mechanical properties of graphene nanopapers are also governed by the annealing temperature because water residuals or organic species existing between nanosheets would be removed during this process, leading to the reduced distance between graphene layers. Note that the van der Vaals or $\pi-\pi$ interactions are highly dependent on the distance between graphene nanosheets, and significantly increase as the distance reduces.[30] It can be observed from Figures 2c, d that the average tensile strength and Young's modulus of graphene nanopapers with 13.7 wt % functional group increased up to 311.9 ± 33.5 MPa and 89.4 ± 8.5 GPa, respectively, as the annealing temperature increased from 60 to 200 °C. However, these properties showed a descendant trend above 200 °C, which may be the consequence of the bubble defects induced by the decomposed SO_2 and CO_2 gases entrained in the nanopapers.

The concentration of functional groups and the annealing temperature also play vital roles in the electrical conductivity of GP−SO_3H nanopapers, as displayed in Figure 4. Specifically, the electrical conductivity

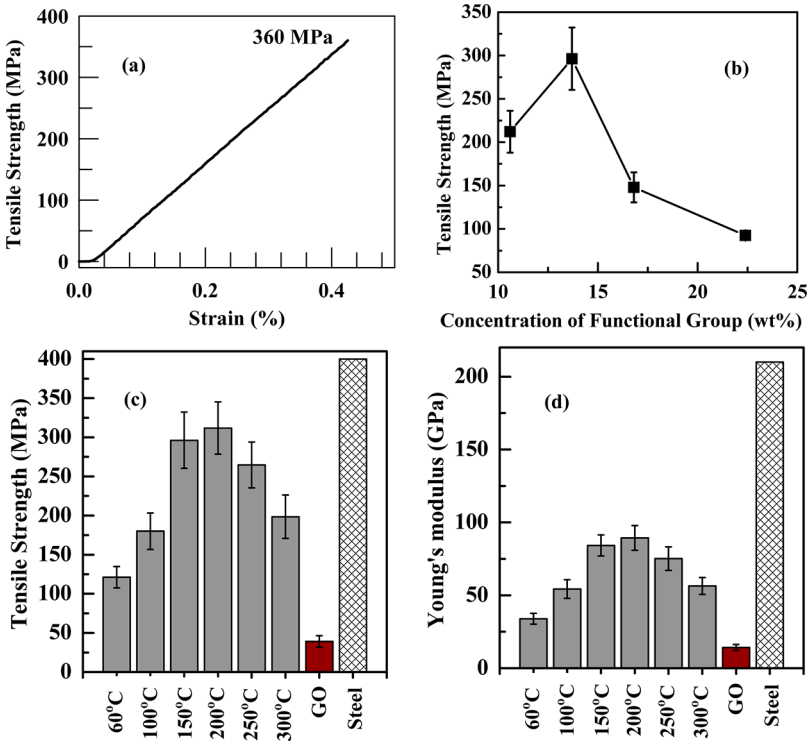

Figure 2. Mechanical properties of nanopapers. (a) Stress−strain curve for the highest tensile strength measured for GP−SO_3H nanopaper with 13.7 wt % functional group annealed at 150 °C for 24 h. (b) Effect of the concentration of functional group on the tensile strength of GP−SO_3H nanopapers after annealing at 150 °C for 24 h. Effect of the annealing temperature on tensile strength (c) and Young's modulus (d) on GP−SO_3H nanopapers with 13.7 wt % functional group, as compared with those of GO nanopaper and structural steel.

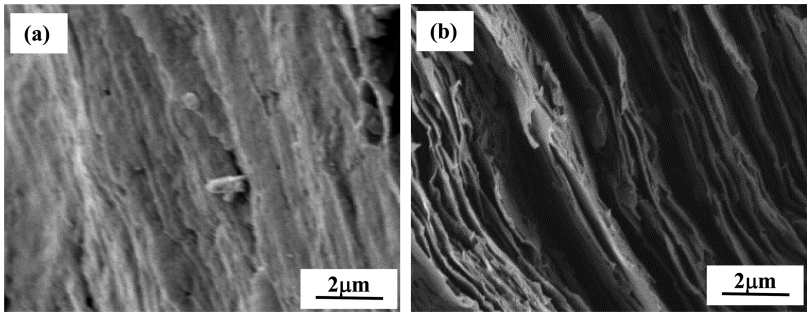

Figure 3. SEM images for the perpendicular surfaces of (a) GP−SO_3H and (b) GO nanopapers after tensile tests.

of nanopapers diminished with the increase of functionality, whereas it showed a reverse trend for the annealing temperature. This is because the covalently bonded functional groups on the graphene would result in sp^3 nodes, interrupting the conducting pathways in the graphene plane and thus decreasing electrical conductivity. Moreover, the interlayer gallery distance in nanopapers would increase if the degree of functionality is raised, resulting in the reduced electrical conductivity due to the decreased contact points between nanosheets. Since the annealing temperature has a positive effect on the distances between graphene nanosheets, a higher annealing temperature is beneficial for electrical conductivity of graphene nanopapers. The electrical conductivity of about 4.45×10^4 S/m was measured for the nanopaper with DS = 1.21 after being annealed at 250 °C, which is more than one-third of that of natural graphite[31] and three times over the reported value of graphene nanopaper under the same annealing condition.[20] This observation can be attributed to the high degree of reduction of our functional graphenes and high quality of our graphene nanopapers.

XPS data provide an insight into the structural change of GP−SO_3H nanopapers during thermal annealing. It can be observed from Figure 5a that the peak of the sulfur element in GP−SO_3H remained unchanged when the annealing temperature was 150 °C, then it greatly reduced at an annealing temperature of 250 °C and completely disappeared at an annealing temperature of 500 °C. This means that a majority of −SO_3H groups in the functional graphenes degraded at temperatures

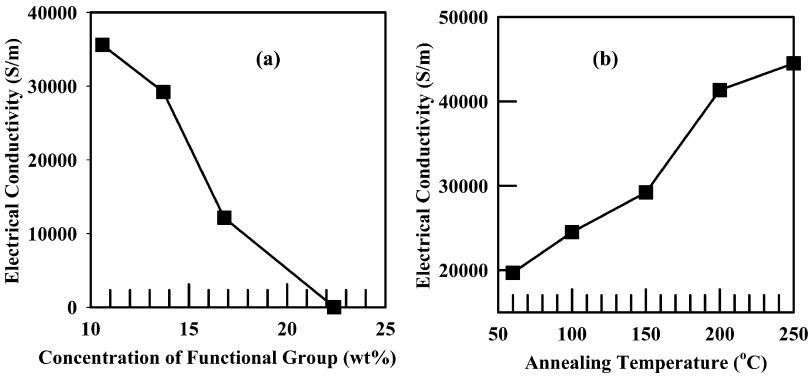

Figure 4. Electrical conductivity of graphene nanopapers. (a) Effect of the concentration of functional group of GP−SO_3H nanopapers annealed at 150 °C and (b) effect of annealing temperature on the electrical conductivity of GP−SO_3H nanopapers with 13.7 wt % functional group.

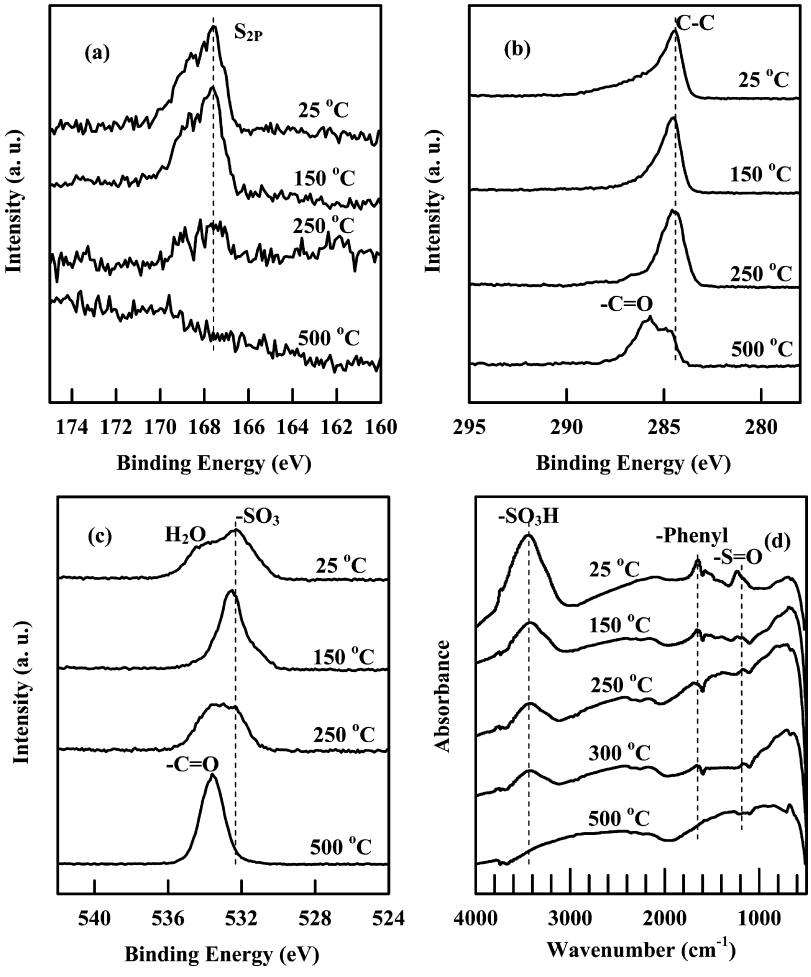

Figure 5. XPS spectra of (a) S_{2p} signal, (b) C(1s) signal, and (c) O(1s) signal, as well as (d) FTIR spectra of GP−SO_3H annealed at different temperatures.

above 250 °C. It can be learned from Supporting Information, Figure S7 that GP−SO_3H only exhibits a peak at 284.4 eV for C−C species, supporting the loss of C−O and C═O functionalities on the surface of graphene by reduction.[32,33] The long tail of the C(1s) signal of the unannealed sample in Figure 5b reflects the presence of water because it would increase the gallery distance between graphene nanosheets. The tail became invisible upon the removal of water at an annealing temperature of 150 °C. As the sample was annealed at 250 °C, a small shoulder exhibited at 287.1 eV, which became very strong at an annealing temperature of 500 °C. This arose from the partial oxidation of carbon element by the decomposed SO_3H at elevated temperatures. Figure 5c shows the O(1s) signal changes of GP−SO_3H nanopapers at various annealing temperatures. A binding

energy peak at 532.6 eV primarily came from the $-SO_3$ in the GP$-SO_3H$ nanopaper, while a shoulder at 533.9 eV indicated the contribution of water to the O(1s) signal for the nanopaper without annealing.[34] This shoulder disappeared as the water was removed upon annealing at 150 °C. As the annealing temperature increased to 250 °C, the number of sulfonic acid groups in GP$-SO_3H$ nanopaper decreased while some of the carbon elements in the graphene were oxidized. As a result, we observed the reduced peak intensity at a binding energy of 532.6 eV for sulfonic acid groups and a new peak at 533.7 eV for C═O groups. At an annealing temperature of 500 °C, the O(1s) signal was predominately assigned to the C═O groups, as a consequence of oxidization of graphenes. This observation is further confirmed by the FTIR spectra in Figure 5d for GP$-SO_3H$ nanopapers annealed at various temperatures.

The FTIR spectra in Figure 5d gives the evidence of $-SO_3H$ at a broad absorption peak ranging from 2850 to 3600 cm^{-1}, a phenyl absorption peak at 1621 cm^{-1}, and a −S═O absortion peak at 1120 cm^{-1}. At room temperature, the water residual in the nanopaper contributes a lot to the absorption peak ranging from 2850 to 3600 cm^{-1}, due to the hydroxyl groups in water molecules. Upon annealing at 150 °C, most of water residual would be removed under vacuum. Thus, we observed a significant reduction in absorption density for this peak after annealing at 150 °C. This absorption peak intensity was slightly reduced when the annealing temperature increased from 150 to 250 °C, meaning that some of $-SO_3H$ groups have been lost due to degradation. This observation is well consistent with those made in XPS spectra in Figure 5a. However, when the annealing temperature was further increased to 300 °C, this absorption peak became fairly small, and completely disappeared when the annealing temperature arrived at 500 °C. These trends can be further confirmed by the change of absorption intensity for the −S═O peak at 1120 cm^{-1} with the annealing temperatures. The intensity of absorption peak at 1621 cm^{-1} began to diminish when the annealing temperature was greater than 300 °C, indicating that − phenyl groups in benzenesulfonic acid would degrade above this temperature. These results agree with our observation that there were bubble-like defects in the nanopapers annealed at temperatures above 250 °C, and these defects became more obvious at higher annealing temperatures because more decomposed gases like SO_2 and CO_2 were entrained inside the nanopaper and the built-up pressure led to bubble formation. Consequently, we observed the reduced mechanical properties as the annealing temperature exceeded 250 °C.

The X-ray diffraction (XRD) patterns of GP$-SO_3H$ nanopapers in Figure 6 are significantly different from those of expanded graphite and graphene oxide[14] in Supporting Information, Figure S8. Specifically, the

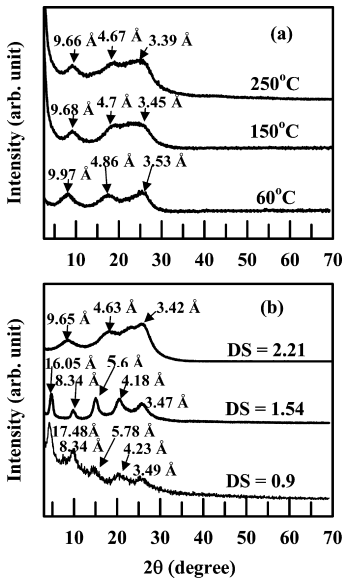

Figure 6. XRD patterns of GP$-SO_3H$ nanopapers. (a) Effect of annealing temperatures for nanopaper with DS = 1.54, and (b) effect of degree of functionality (DS) per 100 carbons after annealing at 150 °C for 24 h.

GP$-SO_3H$ nanopaper with DS = 1.21 annealed at 60 °C in Figure 6a exhibits three reflection peaks with *d*-spacings of 9.97, 4.86, and 3.53 Å, respectively. The first two peaks may be attributed to bulky benzenesulfonic acid groups that increase the gallery distance between graphene nanosheets, while the latter one arises from the $\pi-\pi$ stacking between nanosheets. We have further examined the effect of annealing temperature on the XRD patterns of nanopapers, and have found that the *d*-spacings are gradually lessened with the increase of annealing temperatures. This agrees with our observations in the annealing effects on GP$-SO_3H$ nanopapers *via* XPS spectra and FTIR spectra in Figure 5 that increasing the annealing temperature would remove more water/organic species existing between the nanosheets and thus drive them to pack more tightly. As a result, the mechanical and electrical properties of nanopapers gradually increase with the annealing temperatures below 250 °C.

The effect of concentration of functional groups on the X-ray diffraction patterns of GP$-SO_3H$ nanopapers is illustrated in Figure 6b. For GP$-SO_3H$ with DS = 0.9 after being annealed at 150 °C for 24 h, there exhibits three reflection peaks with *d*-spacings of 9.65, 4.63, and 3.42 Å, respectively. As DS increases to 1.21 in Figure 6a, the *d*-spacings of these three reflection peaks become 9.68, 4.7, and 3.45 Å respectively, due to the increased amount of functional groups. Interestingly, GP$-SO_3H$ nanopaper with DS = 1.54 shows five reflection peaks with *d*-spacings of 16.05, 8.34, 5.6, 4.18, and 3.47 Å, respectively. These peaks are further enlarged to 17.48, 8.34, 5.78, 4.23, and 3.49 Å, respectively for GP$-SO_3H$ nanopaper with DS = 2.21. It is noticeable that the reflection peak at 17.48 Å shows stronger intensity while

the intensity of other reflection peaks attenuated for nanopapers with DS = 2.21. The aforementioned unambiguous evidence verifies the conjecture that the increased number of functional groups on graphenes would give rise to a larger gallery distance between graphene nanosheets, leading to the reduced properties observed in Figures 2b and 4a.

CONCLUSION

In summary, we developed a facile and effective approach to synthesize functional graphenes having benzenesulfonic acid groups that facilitate the dispersion of graphene nanosheets in water and allow the preparation of nanopapers by flow-directed assembly. Both mechanical and electrical properties of graphene nanopapers are sensitive to the annealing temperature and the degree of functionality. We optimized the processing conditions to achieve hydrophobic graphene nanopapers with the highest tensile strength of 360 MPa and Young's modulus of 102 GPa in a sample with 13.7 wt % functional group and annealed at 150 °C and also possessing a high electrical conductivity of 4.45×10^4 S/m for the same sample being annealed at 250 °C, properties much higher than any previous reported data.

METHODS

For the synthesis of 4-sulfonic acid phenyl diazonium tetrafluoroborate, tetrafluoroboric acid (48 wt % aqueous solution, 21.6 mL, 170 mmol) was added dropwise to a suspension of 4-sulfanilic acid (17.8 g, 100 mmol) in 100 mL of distilled water. The mixture was then cooled to 0 °C and a saturated solution of sodium nitrite (7.1 g, 100 mmol) in water was added slowly. During the addition, the temperature was carefully kept below 5 °C. The reaction mixture was stirred for 2 h. The resulting white precipitate was collected by filtration and washed with diethyl ether, followed by freeze-drying and storing in a refrigerator. FTIR spectrum (cm^{-1}): 2920(−CH−), 2850(−CH−), 2306 ($-N_2^+$), 1564, 1400, 1313(−S═O), 1236, 1191, 1168, 1125, 1114(−S═O), 1071, 1028, 997, 830, 819, 700, 652, 551, 517. ^{1}H NMR spectrum (250 MHz, DMSO-d_5, δ/ppm): 8.64 (d, J = 8.5 Hz, 2H, Ar−H), 8.10 (d, J = 8.5 Hz, 2H, Ar−H).

As a typical example for synthesizing GP−SO_3H with DS = 1.21, graphite oxide (1.2 g, about 100 mmol) powder was dispersed in 1000 mL of distilled water and the pH of the mixture was adjusted to about 9 using 5 wt % sodium carbonate aqueous solution. The mixture was then subjected to mild ultrasound for 30 min. During this process, graphite oxide was exfoliated to individual graphene nanosheets to form a stable dispersion of graphene oxide solution. The obtained solution was centrifuged at 2000 rpm for 30 min to remove any trace of unreacted graphite. The solution of graphene oxide was then partially reduced using sodium borohydride (7.8 g, 200 mmol) in 100 mL of distilled water at 70 °C for 1 h. The resulting suspension was filtered off and washed with distilled water until the pH value reached 7. The obtained partially reduced graphene oxide was redispersed in 1000 mL of distilled water under mild sonication for 30 min, and then cooled down to room temperature using an ice bath. A solution of 4-sulfonic acid phenyl diazonium tetrafluoroborate (1.36 g, 5 mmol) in 10 mL of distilled water was added dropwise to the partially reduced graphene oxide solution, and stirred at this temperature for 6 h. The reaction solution was sonicated for 30 min, and then the second portion of 4-sulfonic acid phenyl diazonium tetrafluoroborate (1.36 g, 5 mmol) was applied according to the aforementioned procedures. Upon the completion of the reaction, 5 wt % sodium carbonate aqueous solution was added to adjust the pH value of the solution to above 10, during which precipitates were formed. The precipitates were filtered off and washed with water and ethanol to form GO−SO_3H. Subsequently, GO−SO_3H was redispersed in 1000 mL of distilled water and then fully reduced to GP−SO_3H using hydrazine hydrate (50−60%, 32 mL) at 100 °C for 24 h, during which the presence of sulfonic acid would keep graphenes in good dispersion in water. After the reaction was finished, the pH value of the reaction solution was adjusted to above 10 using 5 wt % sodium carbonate aqueous solution, and precipitates were filtered off and washed completely with water, and then freeze-dried to give GP−SO_3H (1.19 g).

Preparation of Graphene Nanopapers. A predetermined amount of GP−SO_3H was dispersed in water, sonicated in a batch sonicator, and then centrifuged at 2000 rpm to remove any insoluble impurity. Nanopapers with different thicknesses ranging from several hundred nanometers to 30 μm were prepared by filtration of the graphene solution through a polycarbonate membrane filter with a pore size of 400 nm, followed by air drying. The free-standing graphene nanopapers were obtained by peeling them off from the filter, and then annealing at different temperatures in a vacuum oven for 24 h. GO nanopapers were prepared according to the literature.[14]

Characterizations of Functional Graphenes and Nanopapers. ^{1}H NMR spectra were obtained on a Bruker DPX 250 spectrometer at 298 K. Chemical shifts (δ) were reported in ppm relative to the signal of tetramethylsilane (TMS). Residual solvent signals in the ^{1}H spectra were used as an internal reference. Coupling constants (J) were given in Hz. Atomic force microscope (AFM) images were taken in the tapping mode with Asylum MFP-3D AFM. Fourier transform infrared (FTIR) spectra were recorded on a Thermo Nicolet 380 FTIR spectrometer (Thermo Fisher Scientific) with a diamond attenuated total reflectance (ATR) accessory. Thin films suitable for FTIR spectroscopy were prepared by casting an aqueous solution (0.3 mg/mL) of GP−SO_3H directly on the KBr salt plate. X-ray photoelectron spectroscopy (XPS) was carried out on a Kratos Axis Ultra XPS instrument equipped with both monochromated (Al) and dual (Mg and Al) X-ray guns set at 10 mA, 12 kV, and pass energy of 80 eV for high-resolution scan (5×10^{-9} Torr). The magnification gave an analysis area of 700 μm by 300 μm. The Raman spectra were recorded using a Renishaw inVia Raman microscope with an excitation wavelength of 514.5 nm. The X-ray diffraction (XRD) patterns were determined on a Scintag XDS-2000 X-ray diffractometer equipped with an intrinsic germanium detector system using Cu Kα radiation (λ = 1.5418 Å), operated at 45 kV and 20 mA. The morphology of graphene nanopapers was observed using a scanning electron microscope (SEM, PhilipsXL30). The mechanical properties of nanopapers were measured on a dynamic mechanical analyzer (RSA III, TA Instruments) in the controlled strain rate mode. The specimens were cut with a razor into rectangular strips with a width of 5 mm and a length of 30 mm. The thickness of a specimen was determined from the SEM image of the perpendicular fractured surface. Eight measurements were conducted for each sample, and the results were averaged. The electrical conductivity was measured by the Van Der Pauw method with a Keithley 6514 electrometer.

Conflict of Interest: The authors declare no competing financial interest.

Supporting Information Available: Reaction scheme, TGA, contact angle, Raman spectra, and XRD patterns of graphenes and nanopapers. This material is available free of charge *via* the Internet at http://pubs.acs.org.

REFERENCES AND NOTES

1. Olek, M.; Ostrander, J.; Jurga, S.; Möhwald, H. K., N.; Kempa, K.; Giersig, M. Layer-by-Layer Assembled Composites from Multiwall Carbon Nanotubes with Different Morphologies. *Nano Lett.* **2004**, *4*, 1889–1895.

2. Mamedov, A. A.; Kotov, N. A.; Prato, M.; Guldi, D. M.; Wicksted, J. P.; Hirsch, A. Molecular Design of Single-Wall Carbon Nanotube/Polyelectrolyte Multilayer Composites. *Nat. Mater.* **2002**, *1*, 190–194.
3. Mowa, S.; Ouyang, X.; Castro, J.; Lee, L. J. Carbon Nanofiber Paper and Its Effect on Cure Kinetics of Low Temperature Epoxy Resin. *J. Appl. Polym. Sci.* **2012**, *125*, 2223–2230.
4. Podsiadlo, P.; Kaushik, A. K.; Arruda, E. M.; Waas, A. M.; Shim, B. S.; Xu, J.; Nandivada, H.; Pumplin, B. G.; Lahann, J.; Ramamoorthy, A.; *et al*. Ultrastrong and Stiff Layered Polymer Nanocomposites. *Science* **2007**, *318*, 80–83.
5. Hendriksson, M.; Berglund, L. A.; Isaksson, P. L.; Lindström, T.; Nishino, T. Cellulose Nanopaper Structures of High Toughness. *Biomacromolecules* **2008**, *9*, 1579–1585.
6. Li, D.; Müller, B.; Gilje, S.; Kaner, R. B.; Wallace, G. G. Processable Aqueous Dispersions of Graphene Nanosheets. *Nat. Nanotechnol.* **2008**, *3*, 101–105.
7. Ranjbartoreh, A. R.; Wang, B.; Shen, X.; Wang, G. Advanced Mechanical Properties of Graphene Paper. *J. Appl. Phys.* **2011**, *109*, 014306.
8. Kim, H.; Abdala, A. A.; Macosko, C. W. Graphene/Polymer Nanocomposites. *Macromolecules* **2010**, *43*, 6515–6530.
9. Ray, S. S.; Okamoto, M. Polymer/Layered Silicated Nanocomposites: A Review from Preparation to Processing. *Prog. Polym. Sci.* **2003**, *28*, 1539–1641.
10. Lee, C.; Wei, X. D.; Kysar, J. W.; Hone, J. Measurement of the Elastic Properties and Intrinsic Strength of Monolayer Graphene. *Science* **2008**, *321*, 385–388.
11. Kane, C. L. Materials Science: Erasing Electron Mass. *Nature* **2005**, *438*, 168–170.
12. Balandin, A. A.; Ghosh, S.; Bao, W. Z.; Calizo, I.; Teweldebrhan, D.; Miao, F.; Lau, C. N. Superior Thermal Conductivity of Single-Layer Graphene. *Nano Lett.* **2008**, *8*, 902–907.
13. Zhu, Y.; Murali, S.; Cai, W.; Li, X.; Suk, J. W.; Potts, J. R.; Ruoff, R. S. Graphene and Graphene Oxide: Synthesis, Properties, and Applications. *Adv. Mater.* **2010**, *22*, 3906–3924.
14. Dikin, D. A.; Stankovich, S.; Zimney, E. J.; Piner, R. D.; Dommett, G. H. B.; Evmenenko, G.; Nguyen, S. T.; Ruoff, R. S. Preparation and Characterization of Graphene Oxide Paper. *Nature* **2007**, *448*, 457–460.
15. Stankovich, S.; Dikin, D. A.; Piner, R. D.; Kohlhaas, K. A.; Kleinhammes, A.; Jia, Y.; Wu, Y.; Nguyen, S. T.; Ruoff, R. S. Synthesis of Graphene-Based Nanosheets *via* Chemical Reduction of Exfoliated Graphite Oxide. *Carbon* **2007**, *45*, 1558–1565.
16. Lomeda, J. R.; Doyle, C. D.; Kosynkin, D. V.; Hwang, W.-F.; Tour, J. M. Diazonium Functionalization of Surfactant-Wrapped Chemically Converted Graphene Sheets. *J. Am. Chem. Soc.* **2008**, *130*, 16201–16206.
17. Coleman, J. N. Liquid-Phase Exfoliation of Nanotubes and Graphene. *Adv. Funct. Mater.* **2009**, *19*, 3680–3695.
18. Lotya, M.; Hernandez, Y.; King, P. J.; Smith, R. J.; Nicolosi, V.; Karlsson, L. S.; Blighe, F. M.; De, S.; Wang, Z.; McGovern, I. T.; *et al*. Liquid Phase Production of Graphene by Exfoliation of Graphite in Surfactant/Water Solution. *J. Am. Chem. Soc.* **2009**, *131*, 3611–3620.
19. Lotya, M.; King, P. J.; Khan, U.; De, S.; Coleman, J. N. High-Concentration, Surfactant-Stabilized Graphene Dispersions. *ACS Nano* **2010**, *4*, 3155–3162.
20. Chen, H.; Müller, M. B.; Gilmore, K. J.; Wallace, G. G.; Li, D. Mechanically Strong, Electrically Conductive, and Biocompatible Graphene Paper. *Adv. Mater.* **2008**, *20*, 3557–3561.
21. Dong, Z.; Jiang, C.; Cheng, H.; Zhao, Y.; Shi, G.; Jiang, L.; Qu, L. Facile Fabrication of Light, Flexible and Multifunctional Graphene Fibers. *Adv. Mater.* **2012**, *24*, 1856–1861.
22. Si, Y.; Samulski, E. T. Synthesis of Water Soluble Graphene. *Nano Lett.* **2008**, *8*, 1679–1682.
23. Staudenmaier, L. Verfahren zur Darstellung der graphitsäure. *Ber. Dtsch. Chem. Ges.* **1898**, *31*, 1481–1487.
24. McAllister, M. J.; Li, J.-L.; Adamson, D. H.; Schniepp, H. C.; Abdala, A.; Liu, J.; Herrera-Alonso, M.; Milius, D. L.; Car, R.; Prud'homme, R. K.; *et al.* Single Sheet Functionalized Graphene by Oxidation and Thermal Expansion of Graphite. *Chem. Mater.* **2007**, *19*, 4396–4404.
25. Bahr, J. L.; Yang, J.; Kosynkin, D. V.; Bronikowski, M. J.; Smalley, R. E.; Tour, J. M. Functionalization of Carbon Nantotubes by Electrochemical Reduction of Aryl Diazonium Salts: A Bucky Paper Electrode. *J. Am. Chem. Soc.* **2001**, *123*, 6536–6542.
26. Sinitskii, A.; Dimiev, A.; Corley, D. A.; Fursina, A. A.; Kosynkin, D. V.; Tour, J. M. Kinetics of Diazonium Functionalization of Chemically Converted Graphene Nanoribbons. *ACS Nano* **2010**, *4*, 1949–1954.
27. Kudin, K. N.; Ozbas, B.; Schniepp, H. C.; Prud'homme, R. K.; Aksay, I. A.; Car, R. Raman Spectra of Graphite Oxide and Functionalized Graphene Sheets. *Nano Lett.* **2008**, *8*, 36–41.
28. Pimenta, M. A.; Dresselhaus, G.; Dresselhaus, M. S.; Cancado, L. G.; Jorio, A.; Saito, R. Studying Disorder in Graphite-Based Systems by Raman Spectroscopy. *Phys. Chem. Chem. Phys.* **2007**, *9*, 1276–1291.
29. Ni, Z.; Wang, Y.; Yu, T.; Shen, Z. Raman Spectroscopy and Imagning of Graphene. *Nano Res.* **2008**, *1*, 273–291.
30. Rozploch, F.; Patyk, J.; Stankowski, J. Graphenes Bonding Forces in Graphite. *Acta Phys. Pol., A* **2007**, *112*, 557–562.
31. Deprez, N.; McLachlan, D. S. The Analysis of the Electrical Conductivity of Graphite Conductivity of Graphite Powders During Compaction. *J. Phys. D: Appl. Phys.* **1988**, *21*, 101.
32. Yang, D.; Velamakanni, A.; Bozoklu, G.; Park, S.; Stroller, M.; Piner, R. D.; Stankovich, S.; Jung, I.; Field, D. A.; Ventrice, C. A. J.; *et al*. Chemical Analysis of Graphene Oxide Films after Heat and Chemical Treatments by X-ray Photoelectron and Micro-Raman Spectroscopy. *Carbon* **2009**, *47*, 145–152.
33. Choudhury, D.; Das, B.; Sarma, D. D.; Rao, C. N. R. XPS Evidence for Molecular Charge-Transfer Doping of Graphene. *Chem. Phys. Lett.* **2010**, *497*, 66–69.
34. Yamamoto, S.; Bluhm, H.; Andersson, K.; Ketteler, G.; Ogasawara, H.; Salmeron, M.; Nilsson, A. *In Situ* X-Ray Photoelectron Spectroscopy Studies of Water on Metals and Oxides at Ambient Conditions. *J. Phys.: Condens. Matter* **2008**, *20*, 184025.